ACS OMEGA

http://pubs.acs.org/journal/acsodf

Article

Kinetic Analysis of Devolatilized Diesel-Soot Oxidation Catalyzed by Ag/Al_2O_3 and Ag/CeO_2 Using Isoconversional and Master-Plots Techniques

Boonlue Sawatmongkhon, Punya Promhuad, Thanawat Thaisruang, Kampanart Theinnoi,* Sak Sittichompoo, Thawatchai Wongchang, and Ekarong Sukjit

Cite This: *ACS Omega* 2023, 8, 29437−29447

Read Online

ACCESS | Metrics & More | Article Recommendations

ABSTRACT: This work presented the kinetic analysis of devolatilized diesel-soot combustion accelerated by Ag/Al_2O_3 and Ag/CeO_2 catalysts. Isoconversional and master-plots techniques were employed to estimate activation energy and identify the reaction model. The apparent activation energy of uncatalyzed soot oxidation was 101.85 kJ/mol, and it was reduced to 61.85 and 82.78 kJ/mol for the combustion catalyzed by Ag/Al_2O_3 and Ag/CeO_2, respectively. The reaction-order model, $f(\alpha) = (1-\alpha)n$, with n of 1.4, 1, and 1 showed the best fit for the uncatalyzed soot oxidation and soot oxidation catalyzed by Ag/Al_2O_3 and Ag/CeO_2, respectively. The proposed single-step reaction models were quite capable of reproducing experiments for the uncatalyzed soot oxidation and soot oxidation catalyzed by Ag/CeO_2. In the presence of Ag/Al_2O_3, the oxidation rate at the first 20% of conversion was faster than the 1st-order reaction reflecting that the soot was rapidly oxidized by highly active species generated by Ag/Al_2O_3. The oxidation of the remaining soot closely followed the 1st-order reaction mechanism.

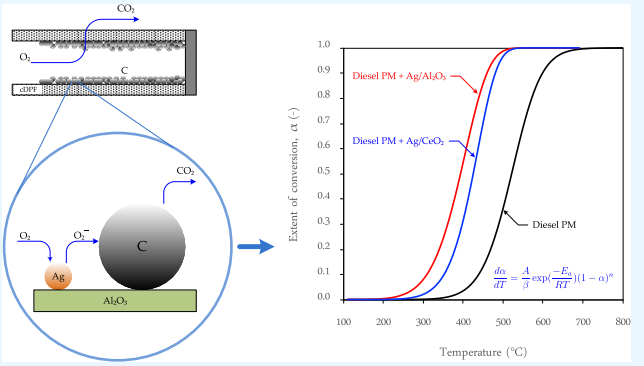

1. INTRODUCTION

The removal of particulate matter (PM) contained in the diesel-engine exhaust has gained attention worldwide. The most promising solution for the diesel-PM (DPM) problem is using a diesel particulate filter (DPF). There are two consecutive steps for DPF to remove PM from the exhaust. First, DPM is entrapped on the wall of DPF, called filtering. Next, the accumulated DPM is periodically removed by burning into CO_2, denoted as filter regeneration. Therefore, the function of DPF is completely recovered and ready for use in the next cycle. Typically, the regeneration process starts at the temperature of 550−600 °C when oxygen is used as the oxidizer. In contrast, in the presence of NO_2, the combustion process is initiated at 300−350 °C. Unfortunately, a modern diesel engine is generally designed to produce a low NO_x concentration that reduces the opportunity to use NO_2 as the oxidizer. Direct oxidation of DPM is not suitable for DPF regeneration because it requires a high temperature (~600°C[1]), while the temperature of diesel exhaust gas is in a range of 180−400 °C.[2,3] Alternatively, catalytic regeneration of DPF by coating a catalyst material on filter walls is favorable due to its low reaction temperature. Generally, catalytic DPM oxidation depends strongly on the catalyst used. Therefore, several active metals, support materials, and promoters have been studied. Oxidation catalysts are often made from noble metals like platinum, ruthenium, palladium, gold, and rhodium which are costly. A silver (Ag)-supported catalyst is a more cost-effective alternative. It shows the remarkable promotion of PM oxidation.[1,4−12] Corro et al.[13] studied the promotion of Ag/SiO_2 (insulator) and Ag/ZnO (semiconductor) to the catalytic combustion of DPM using the X-ray photoelectron spectroscopy (XPS) technique. Ag/SiO_2 showed excellent DPM oxidation at the temperature below 300 °C due to the presence of a metallic state of Ag (Ag^0) on the SiO_2 surface. Ag^0 facilitated the generation of superoxide (O_2^-) which was a highly active oxidizer for the combustion of DPM. Furthermore, the catalyst was quite stable as its performance did not change for 6 cycles of DPM oxidation. Previous work from our group found that Ag/Al_2O_3 gave higher DPM

Received: April 30, 2023
Accepted: July 20, 2023
Published: August 2, 2023

oxidation performance than Ag/CeO_2, and it showed high stability for 5 oxidation cycles.[1]

Ag enhances soot oxidation by promoting several processes, for example, the generation of superoxide.[6,7,14,15] After using O_2 temperature-programmed desorption (O_2-TPD), $^{18}O/^{16}O$ isotropic exchange (IE) reaction, and electron spin resonance (ESR) techniques to study the soot oxidation over the rice-ball morphology of the CeO_2-Ag catalyst, Yamazaki et al.[16] proposed a mechanism for soot oxidation. First, atomic oxygen adsorbed weakly on the Ag surface and functioned as the active oxygen species. Next, it migrated to the CeO_2 particles via the extremely large Ag/CeO_2 interface area and transformed later into O_2^- species. Finally, O_2^- further migrated onto soot particles and oxidized efficiently with the particles. Shimizu et al.[4] studied the catalytic behaviors of the silver-loaded ceria catalyst and found that the silver nanoparticle promoted the reducibility of CeO_2, but it did not improve the re-oxidation of reduced CeO_2. The authors suggested a reaction mechanism for soot oxidation on the Ag/CeO_2 catalyst. First, active oxygen species (possibly O_2^-) were formulated from gas-phase O_2 through the chemisorption process on an oxygen vacancy site of CeO_2. Due to the filling of the oxygen into the vacancy site, the oxidation state of ceria was changed from Ce^{3+} to Ce^{4+}. Then, the active oxygen migrated to the surface of carbon and oxidized to produce CO_2. The electronic state of ceria was shifted back to Ce^{3+}, creating an oxygen vacancy site. Under H_2-TPR of CeO_2, there are generally two prominent peaks at approximately 500 and 700 °C, which correspond to the reduction of surface and bulk oxygen of CeO_2, respectively. With doping of Ag onto CeO_2, there is an additional peak at about 200 °C representing the reduction of silver oxides.[6] The active phases usually found in the silver-supported catalyst are Ag_2O and metallic Ag. Ag_2O, which was very active with soot,[4,15] preferred to formulate on the acidic supports (e.g., Ag/Al_2O_3 and Ag/TiO_2), while on the basic supports (e.g., Ag/ZrO_2 and Ag/MgO), the metallic Ag was the major active phase formed.[17] In contrast, metallic Ag was detected on Ag/Al_2O_3 using X-ray diffraction (XRD) by several researchers.[1,18−20] In Ag/ZrO_2, Ag/Al_2O_3, and Ag/CeO_2, Ag_2O was formed first during the catalyst preparation and then it was quickly thermally decomposed into metallic Ag during calcination by forming Ag at the top of Ag_2O. However, with the presence of CeO_2, this process was hindered by the strong interaction between Ag_2O and CeO_2.[18] Shimizu et al.[4] showed that Ag_2O was the most active among 30 kinds of metal oxides for soot oxidation. Nevertheless, its performance was completely lost after the first run, and Ag_2O was permanently changed to metallic Ag. The authors suggested that Ag_2O acted as a strong oxidant not a catalyst. In Ag/CeO_2, the presence of silver led to a decrease in the amount of oxygen vacancy (Ce^{3+}) and weakened the Ce-O bond adjacent to the silver site which, consequently, improved the reducibility of CeO_2 and mobility of surface oxygen.[21] The authors further stated that the reducibility was significantly enhanced in the presence of Ag^{2+} rather than that of Ag^+ or Ag^0. After conducting a cycled H_2-TPR of Ag/CeO_2, Liu et al.[10] suggested that Ag facilitated the generation of superoxide (O_2^-) from the gas-phase O_2. First, atomic oxygen was formed on the Ag site via the dissociative adsorption of O_2; next, it migrated over the surface oxygen vacancy of CeO_2, and then, O_x^- was formed through $2O \rightarrow O_2^- \rightarrow 2O^- \rightarrow 2O^{2-}$. Different oxidation states of Ag^0, Ag^+, and Ag^{2+} (corresponding to metallic Ag, Ag_2O, and AgO, respectively) were identified on Ag/TiO_2, while only Ag^0 was observed on Ag/CeO_2.[22] Moreover, the intensity of the oxidation state strongly depended on the crystalline phase of TiO_2 (e.g., anatase, P25, and rutile). The authors showed that AgO was the main silver oxide of Ag/P25 and Ag/rutile, and it was more active than Ag_2O mainly formed on Ag/anatase. Lee et al.[6] investigated the effect of Ag loading (e.g., 2, 5, 10, and 20 wt %) on the soot oxidation of Ag/CeO_2. The authors stated that at the Ag amount of 5 wt %, there were appropriate values of the Ce^{3+}/Ce^{4+} ratio and surface oxygen vacancies which promoted the formation of O_2^- rather than those of O^- and O^{2-}.

Knowledge about the kinetics of DPM oxidation during the regeneration process is of fundamental importance for the design and optimization of an effective DPF. Kinetic analysis of the solid−gas reaction was applied to study the oxidation of carbonaceous PM to obtain a mathematical description of soot burning behavior.[23−29] The kinetics of soot oxidation is a complex gas−solid system and is classified as a heterogeneous reaction which is different from a homogeneous reaction (e.g., gaseous substances). Its reactivity depends spatially on the location within the solid particle.[30] Both single-step and multi-step reaction mechanisms were used in kinetic analysis to explain processes taking place during the combustion. Gross et al.[31] studied the kinetics of soot oxidation catalyzed by CeO_2 and found that there was no one-step global model that can reproduce the experimental results. The authors successfully modeled soot combustion by detailing the process taking place on the CeO_2 surface in the form of a five-step consecutive reaction model. The kinetic analysis generally evaluates the pre-exponential factor, activation energy, and reaction model (called kinetic triplet). The isoconversional method (also called the model-free method) is one of the techniques used to determine the kinetic triplet. This method is based on the basic idea that at a constant extent of conversion, the reaction rate varies only with the temperature. Its advantage is that a priori knowledge about the reaction model is not necessary to evaluate the apparent activation energy.[32] The master-plots technique is usually applied to identify the reaction model once the apparent activation energies are previously evaluated. It is simple to implement and does not require a complicated mathematical formulation. Therefore, it was widely used especially in the kinetic analysis of lignocellulosic biomass pyrolysis.[33−36]

In this work, kinetic analysis of devolatilized diesel-soot oxidation uncatalyzed and catalyzed by Ag/Al_2O_3 and Ag/CeO_2 was proposed. The apparent activation energy and reaction model were evaluated based on the isoconversional and master-plots techniques, respectively. The pre-exponential factor was determined by optimizing the model with experimental data. The obtained kinetics can be used to predict the catalytic soot combustion which is necessary for designing, controlling, and optimizing the regeneration process of catalytic DPF.

2. EXPERIMENTAL SECTION

2.1. Material Preparation. The silver loaded on Al_2O_3 and CeO_2 supports was prepared via the method of incipient wetness impregnation. Silver nitrate (THOMAS BAKER) of 252 and 79 mg was dissolved in 0.5 cm^3 of distilled water and added dropwise to 1 g of powdered alumina (KEMAUS, BET of 142 m^2/g) and cerium (IV) oxide (Aldrich, 99.9% trace metals basis) to obtain metal loadings of 16 and 5 wt % for Ag/

https://doi.org/10.1021/acsomega.3c02971
ACS Omega 2023, 8, 29437−29447

Al_2O_3 and Ag/CeO_2, respectively. The solvent was removed by drying at 110 °C for 8 h in an oven. The dry sample was then calcined in static air at 600 °C for 2 h.

DPM was directly taken from the exhaust gas of a traditional diesel engine fueled with a mixture of diesel fuel and biodiesel (palm oil) of 7 vol %. The engine was operated at a speed of 1000−2000 rpm and a maximum load of 25−75%. A stainless-steel mesh was rolled at one round and placed inside the exhaust pipe (50 mm ID); then, the trapped PM was collected and dried in a furnace at 110 °C for 8 h. To avoid a complication to the kinetic analysis caused by multi-components contained in DPM, volatile organic compounds (VOCs) were removed by pre-treatment in a flow of pure N_2 (100 cm^3/min) at 550 °C for 2 h. The obtained diesel soot was kept in an airtight container for later experiments.

2.2. Catalyst Characterization. XRD analysis was performed to identify the crystalline structure of the prepared catalysts using a BRUKER D2 PHASER X-ray diffractometer. Cu-Kα radiation (λ = 0.15406 nm) was used as an X-ray source at 30 kV and 10 mA with $10° \leq 2\theta \leq 90°$, a step size of 0.02°, and a scan speed of 1.2°/min. A temperature-programmed reduction (TPR) profile was obtained using the Micromeritics ChemiSorb 2750. The catalyst of 60 mg was placed inside the U-shape tube and flushed by pure He at 80 °C for 30 mins. Then, the temperature was ramped to 850 °C with a heating rate of 10 °C/min under a 30 mL/min of 10 vol % H_2 in Ar. The H_2 consumption was monitored continuously using a thermal conductivity detector (TCD).

2.3. Catalytic Tests. Thermogravimetric analysis (TGA) was performed using a PerkinElmer Pyris 1 (accuracy better than 0.02%) to investigate the catalytic oxidation performance of catalysts. The catalyst and PM with a weight ratio of 5:1 were tightly mixed in a stainless-steel mortar. Then, the mixture (≈10 mg) was placed in a ceramic crucible (6 and 2 mm in bed diameter and depth, respectively) and heated from room temperature to 700 °C at heating rates of 2, 4, 6, and 8 °C/min. This range of heating rates was suitable for preventing temperature gradients on the sample.[37] The sample was not diluted with an inert material. To avoid the effect of oxygen content variation, a constant concentration of oxygen (99.99%) was supplied as the oxidizer with a constant flow rate of 50 cm^3/min. These experimental conditions were suggested to avoid the mass-transfer limitation.[38−40] The change of sample weight with temperature was recorded continuously. One experimental condition was randomly selected to repeat three times to verify the reproducibility. The results showed that the maximum error was less than 1%.

2.4. Kinetic Analysis. The reaction rate of a solid−gas reaction under isothermal conditions can be expressed as

$$\frac{d\alpha}{dt} = A \exp\left(\frac{-E_a}{RT}\right) f(\alpha) \tag{1}$$

According to recommendations from the ICTAC Kinetics Committee, it can be stated that multiple heating rate programs are highly recommended for the calculation of reliable kinetic parameters.[32] Under a heating rate, β, the reaction rate can be rewritten by

$$\frac{d\alpha}{dT} = \frac{A}{\beta}\exp\left(\frac{-E_a}{RT}\right) f(\alpha) \tag{2}$$

A and E_a are the pre-exponential factor and apparent activation energy, respectively, R is the universal gas constant, and T is the absolute temperature. The extent of conversion, α, is the mass fraction of soot burned and evaluated as

$$\alpha = \frac{m_0 - m}{m_0 - m_f} \tag{3}$$

m is the instantaneous mass of soot, m_0 is the initial mass, and m_f is the final mass. The reaction model, $f(\alpha)$, illustrates the availability of the internal surface and structural change of a solid substance as the reaction proceeds.[41] Rearranging and integrating eq 2 with respect to α and T, the following can be obtained:[38]

$$g(\alpha) = \int_0^\alpha \frac{1}{f(\alpha)} d\alpha = \frac{A}{\beta}\int_{T_0}^{T_\alpha} \exp\left(\frac{-E_a}{RT}\right) dT = \frac{AE_a}{\beta R} p(x) \tag{4}$$

The derivation of eq 4 was explained in detail in refs 41, 42. Common reaction models and their integral formulas, $g(\alpha)$, were given in several publications.[32,38,41,43] The integral isoconversional technique, as shown in eq 4, is more appropriate than its counterpart, the differential isoconversional method, for the TGA data since it is not sensitive to random noise.[44] $x = E_a/RT$ and $p(x)$ is the exponential integral. Unfortunately, the $p(x)$ term has no analytical solution; its value can be estimated by a variety of approximations. By using the method of Kissinger−Akahira−Sunose (KAS) (which $p(x) = \exp(-x)/x^2$) associated with optimized parameters proposed by Starink,[45] the modified KAS is presented as

$$\ln\left(\frac{\beta}{T^{1.92}}\right) = \text{constant} - 1.0008\left(\frac{E_a}{RT}\right) \tag{5}$$

With this formula, E_a of a selected α can be estimated easily using the linear plot of $\ln\left(\frac{\beta}{T^{1.92}}\right)$ against $1/T$. A wide range of α (0.05−0.95) with a step not larger than 0.05 are recommended by Vyazovkin et al.[32] The modified KAS gives a considerable improvement in the accuracy of the apparent activation energy compared to the most popular Flynn−Wall−Ozawa (FWO) method, and it is entirely adequate for most practical purposes.[32,37,46]

With prior knowledge of activation energy, the reaction model, $f(\alpha)$, can be identified using the master-plots technique.[33,34,36,38,47−50] The master plot is a characteristic curve that depends only on the reaction model. By choosing α = 0.5 as a reference point, $g(\alpha)/g(0.5)$ in eq 4 can be reduced to

$$\frac{g(\alpha)}{g(0.5)} = \frac{p(x)}{p(x_{0.5})} \tag{6}$$

The suitable $g(\alpha)$ can be selected from the best fit of $\frac{g(\alpha)}{g(0.5)}$ of a standard reaction model compared to the experimental $\frac{p(x)}{p(x_{0.5})}$.[47]

3. RESULTS AND DISCUSSION

3.1. Catalyst Characterization. Figure 1 shows the diffractograms of prepared catalysts. The crystalline planes of metallic Ag at 38.2° (1 1 1), 44.4° (2 0 0), and 64.5° (2 2 0) are found on both Ag/Al_2O_3 and Ag/CeO_2 while the metallic

https://doi.org/10.1021/acsomega.3c02971
ACS Omega 2023, 8, 29437−29447

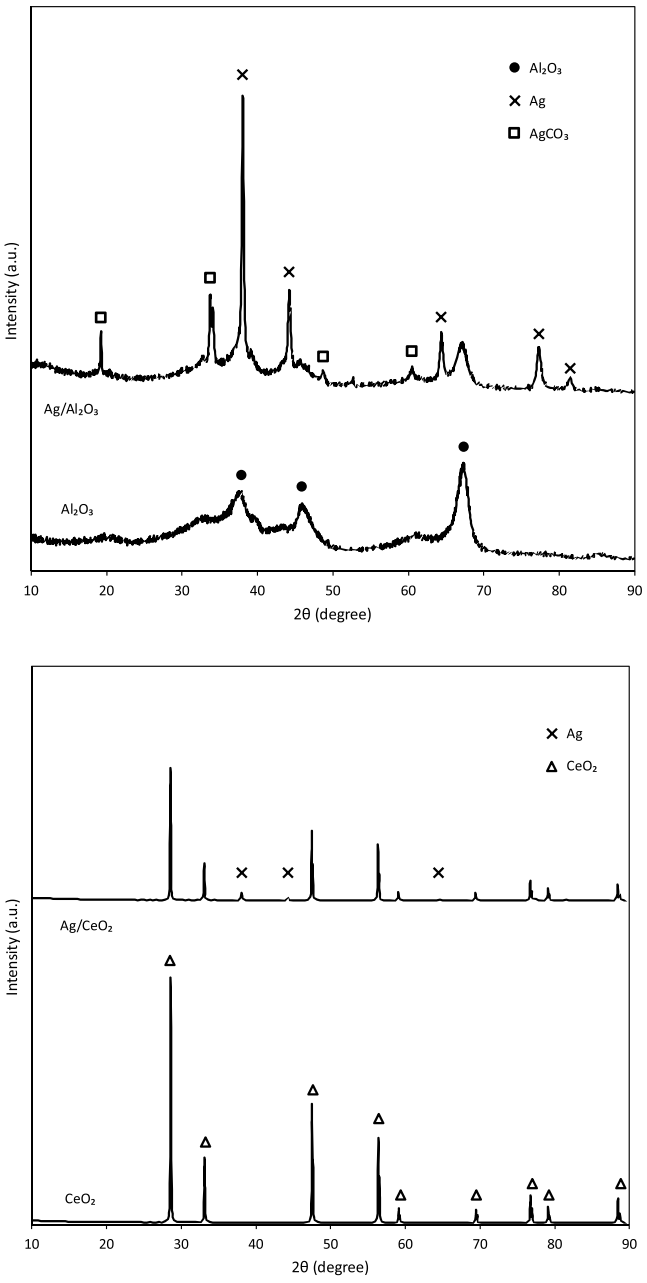

Figure 1. XRD patterns of Al_2O_3, Ag/Al_2O_3, CeO_2, and Ag/CeO_2.

Ag planes at 77.3° (3 1 1) and 81.4° (2 2 2) are detected only on Ag/Al_2O_3. Aneggi et al.[18] showed that, in the XRD results, there were three peaks identified at 38.2, 44.4, and 64.5°, which represented (1 1 1), (2 0 0), and (2 2 0) planes of metallic Ag, respectively. In contrast, our previous work evidenced that, at relatively high Ag contents (8 and 16 wt %), there were two additional peaks detected at 77.3 and 81.4° representing the (3 1 1) and (2 2 2) planes.[1] Small peaks of Ag for Ag/CeO_2 indicating a good dispersion of Ag result in a relatively small crystalline size of Ag. In contrast, the relatively high peaks of Ag for Ag/Al_2O_3 reveal that the large size of Ag is formed on Al_2O_3. The difference in crystal size of Ag is derived from the difference in the Ag content at the step of catalyst preparation (Ag 16 and 5 wt % for Ag/Al_2O_3 and Ag/CeO_2, respectively). Ag_2O is not detected by XRD following the suggestion that Ag_2O is formed during the catalyst preparation and thermally decomposed into metallic Ag during calcination.[18] The fluorite-like structure of CeO_2 presents the peaks (planes) at 28.5° (1 1 1), 33.1° (2 0 0), 47.5° (2 2 0), 56.3° (3 1 1), 59.1° (2 2 2), 69.3° (4 0 0), 76.6° (3 3 1), 79.1 (4 2 0), and 88.5 (4 2 2).

Figure 2 presents H_2-TPR profiles of Ag/Al_2O_3 and Ag/CeO_2. For Ag/Al_2O_3, a distinct reduction peak is detected at

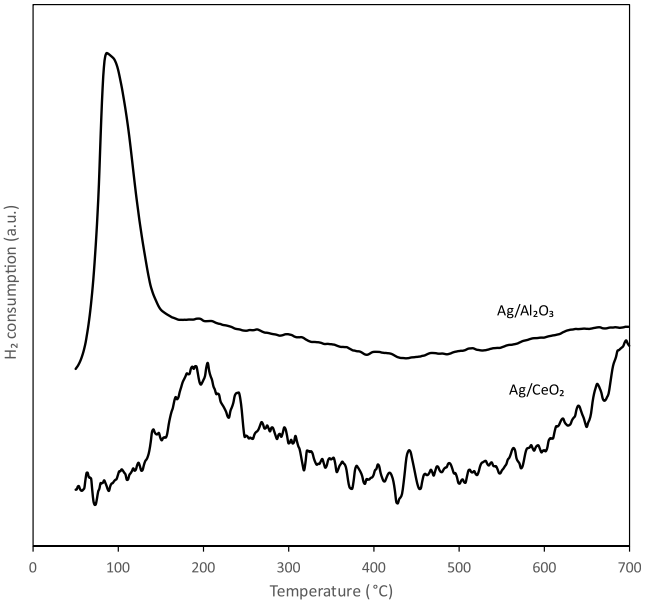

Figure 2. H_2-TPR profiles of Ag/Al_2O_3 and Ag/CeO_2.

100 °C, which corresponds to the reduction of Ag^+ into Ag^0 ($Ag_2O + H_2 \rightarrow 2Ag^0 + H_2O$).[21] This observation is contrary to the study of Aneggi et al.[18] that there was no appearance of a reduction peak of Ag/Al_2O_3 (5 wt % of Ag) for all temperature ranges. The authors proposed that Ag^0 was quickly transformed from Ag_2O by starting the formation of Ag^0 at the top site of Ag_2O. The detection of Ag_2O by H_2-TPR reveals that there is Ag_2O left underneath the metallic Ag. The higher Ag content (16 wt %) in this work causes possibly the difference in H_2-TPR. For the H_2-TPR of Ag/CeO_2, the H_2 consumption peaked at 200 °C indicates the reduction of silver oxides.[6] Another peak is found at the temperature higher than 700 °C (the result not shown), which corresponds to the reduction of bulk oxygen.

3.2. Soot Oxidation in the Absence of a Catalyst.

Figure 3 demonstrates the variation of activation energies on the degree of conversions. The activation energies start from 120 kJ/mol at the beginning of conversion and then slightly decreases with the extent of conversion. These values are normally lower than that obtained from the oxidation of carbon black which is generally used to represent actual DPM. The surrogate soot is more inert than DPM, and its activation energy is in the range of 135−160 kJ/mol depending on the structure of carbon black.[25,26,51,52] A small deviation of the activation energy indicates that the processes taking place during the combustion of pre-treatment DPM are not complex. Therefore, one global step is assumed for the uncatalyzed oxidation of devolatilized DPM. The averaged activation energy of 101.85 kJ/mol is selected to represent the soot combustion. With this activation energy, the reaction model can be identified using the master-plots technique as illustrated in Figure 4. The reaction-order model, $f(\alpha) = (1-\alpha)^n$, with

https://doi.org/10.1021/acsomega.3c02971
ACS Omega 2023, 8, 29437−29447

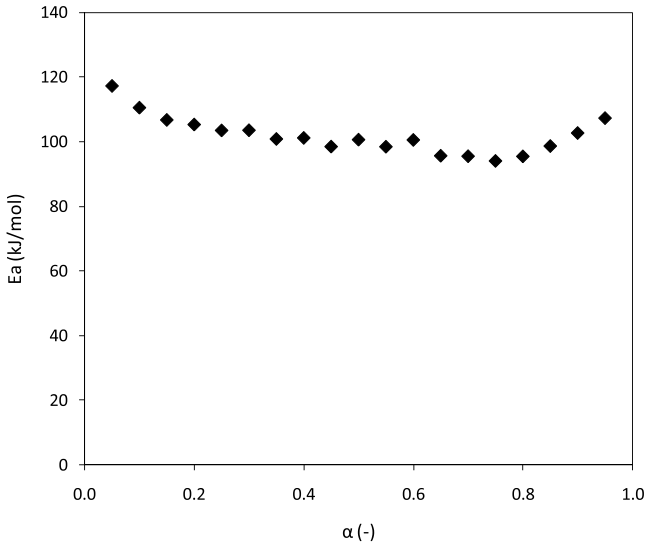

Figure 3. Dependences of the activation energy on the extent of conversion for diesel-soot oxidation in the absence of a catalyst.

the reaction order (n) of 1.4 shows the best fit for the uncatalyzed soot oxidation.

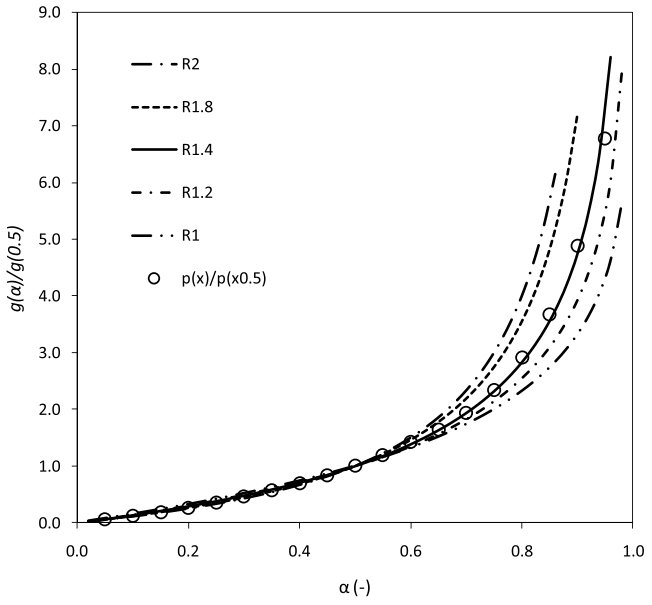

Figure 4. Master plots of $f(\alpha) = (1-\alpha)^n$ and experimental data $p(x)/p(x_{0.5})$ for the uncatalyzed soot combustion at the heating rate of 4 °C/min. R2, R1.8, R1.4, R1.2, and R1 stand for n = 2, 1.8, 1.4, 1.2, and 1, respectively.

With the activation energy and reaction model obtained previously, the pre-exponential factor is estimated by minimizing the error between results from the model and experimental data for all heating rates (using Microsoft Excel). The kinetic triplets obtained are summarized in Table 1.

Figure 5 shows that the reaction-order model with n = 1.4 can successfully reproduce the soot combustion at heating rates of 2, 4, and 6 °C/min for the entire range of soot conversion. It reveals that, in the absence of a catalyst, there is only a primary reaction mechanism taking place during the soot oxidation. Gas-phase oxygen is the only source that provides an oxidizer for combustion. The light-off temperature

Table 1. Activation Energy, Reaction Model, and Pre-Exponential Factor of Soot Oxidation in the Absence of a Catalyst and Presence of Ag/Al_2O_3 and Ag/CeO_2

catalyst	E_a (kJ/mol)	$f(\alpha)$	A (min^{-1})
	101.85	$(1-\alpha)^{1.4}$	306,700
Ag/Al_2O_3	61.85	$1-\alpha$	3290
Ag/CeO_2	82.78	$1-\alpha$	88,910

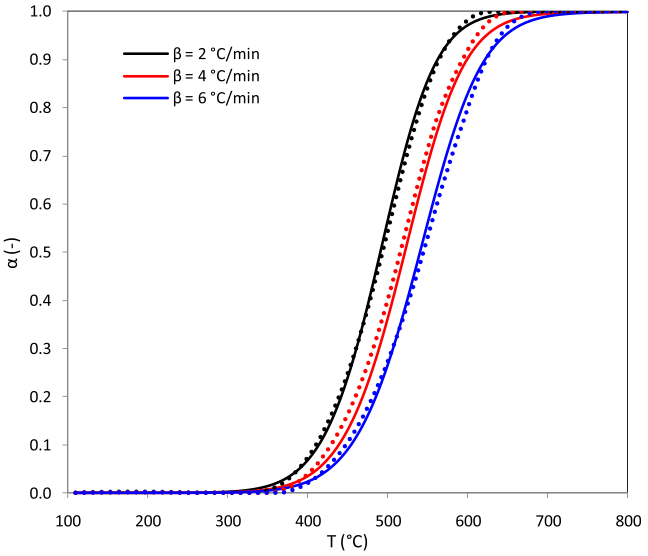

Figure 5. Comparisons between the experiment (dotted lines) and the model (solid lines) at heating rates of 2, 4, and 6 °C/min for the soot combustion in the absence of a catalyst.

of all heating rates is higher than 400 °C, which exceeds the average exhaust temperature of passenger cars. Moreover, the soot combustion takes place between 350 and 650 °C, suggesting that the main components of diesel soot are amorphous and nanofiber carbons which are burned off at 200−500 and 500−600 °C, respectively. The graphitic carbon which combusts between 600 and 800 °C is not found in this work.

The set of parameters shown in Table 1 is used to simulate the soot combustion under different conditions (e.g., at a constant heating rate and an isothermal condition). Figure 6 demonstrates the model performance for soot combustion at different heating rates. The combustion is shifted to a higher temperature when the heating rate increases. The model shows that at the relatively high heating rate, the uncatalyzed soot oxidation is completed at a temperature higher than 700 °C. This temperature level can be reached only by the heat supplied directly from active diesel-fuel burning. Moreover, high temperatures can cause damage to a DPF (e.g., thermal stress).

The effect of a constant temperature on uncatalyzed soot combustion is illustrated in Figure 7. The conversion of soot increases rapidly with the temperature at the beginning and then it proceeds slowly and takes a long time to finish the combustion. The model can predict the time used to complete the soot oxidation. At 650 °C, for example, it takes 30 min to completely burn the soot, while it takes around 2 h at the temperature of 550 °C. This information is necessary to design an active DPF regeneration system by which diesel fuel is added directly to the exhaust gas to increase its temperature. The quantity of fuel and length of injection time can be

https://doi.org/10.1021/acsomega.3c02971
ACS Omega 2023, 8, 29437−29447

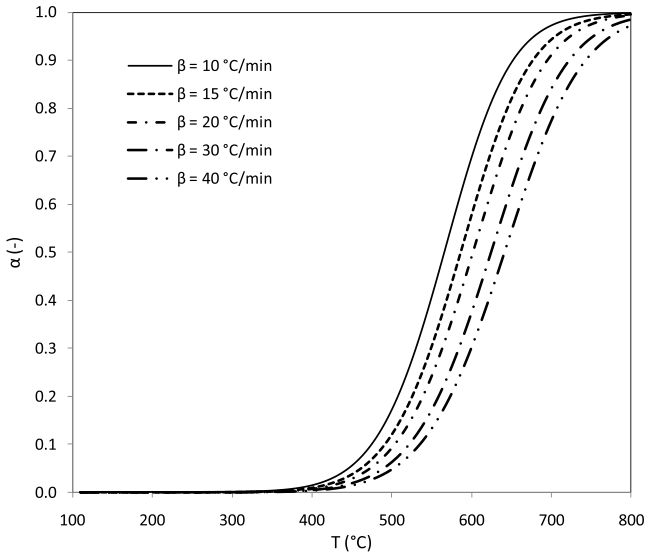

Figure 6. Prediction for the effect of the heating rate on soot combustion in the absence of a catalyst.

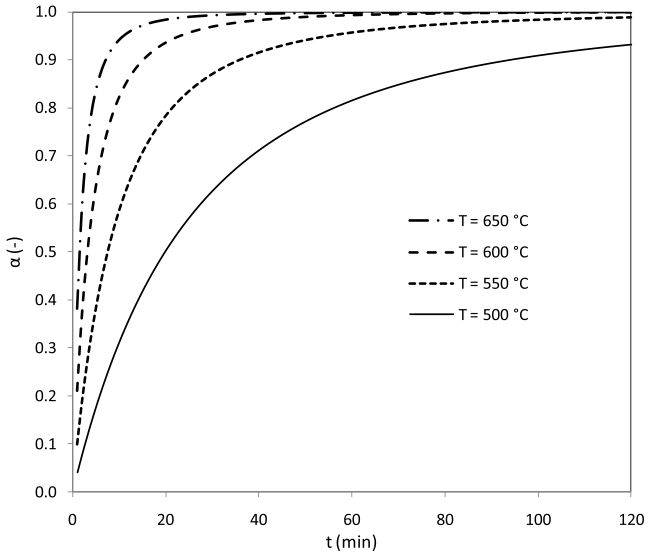

Figure 7. Prediction for the effect of operating temperature on soot combustion in the absence of a catalyst.

estimated using this model to satisfy the design criteria (e.g., too high temperatures are avoided to protect DPF from thermal stress).

3.3. Soot Oxidation in the Presence of Ag/Al_2O_3.

Figure 8 presents the distribution of activation energy of soot oxidation catalyzed by Ag/Al_2O_3. There are relatively low activation energies at the beginning of the combustion process. The activation energies for the entire extent of conversion are in the range of 45−80 kJ/mol. These values are much lower than that of the soot oxidation in the absence of a catalyst which confirms the positive effect of Ag/Al_2O_3 on soot oxidation at all temperature ranges. The significant variation in activation energy with soot conversion states that the soot oxidation accelerated by Ag/Al_2O_3 is complex and consists of several fundamental reaction mechanisms. As mentioned above, the main compositions of devolatilized diesel soot are amorphous and nanofiber carbons. The presence of Ag/Al_2O_3 possibly promotes the decomposition of each component

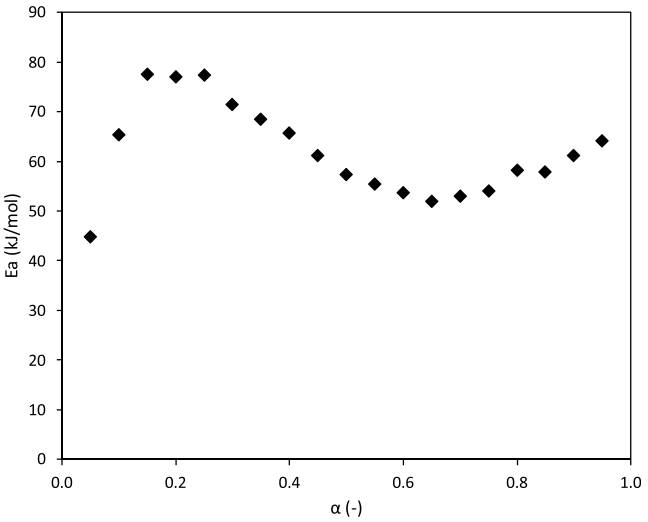

Figure 8. Dependences of the activation energy on the extent of conversion for diesel-soot oxidation in the presence of Ag/Al_2O_3.

through different reaction paths. To model the soot combustion catalyzed by Ag/Al_2O_3 with a single reaction mechanism, the single value of activation energy used in both the master plots and simulation steps is the average of all activation energies, and it is 61.85 kJ/mol.

The master plots of soot combustion catalyzed by Ag/Al_2O_3 are shown in Figure 9. The reaction-order models, $f(\alpha) = (1-\alpha)^n$, of n at 1 and 2 (R1 and R2, respectively) are plotted against the results obtained from the experiment. R1 represents accurately the reaction model of the catalytic oxidation process for the α between 0.2 and 1. However, at the low extent of conversion between 0 and 0.2, the 1st-order reaction model shows a deviation from the experimental data, as illustrated in Figure 9b. This indicates that on Ag/Al_2O_3, the reaction mechanism at the beginning is different from the remaining part of soot combustion. According to the H_2-TPR (Figure 2), there is surface oxygen desorbing from Ag/Al_2O_3 at 50−150 °C in the absence of soot. However, in the presence of soot, this oxygen is not desorbed, but it migrates from the catalyst to soot at low temperatures and oxidizes with soot later at temperatures of 120−350 °C, as displayed in Figure 10.

Figure 10 compares the results obtained from the model with the experiment. The model can accurately reproduce the catalytic combustion of soot in the range of α between 0.2 and 1. As mentioned above, at the low soot conversion (less than 20%), there is a soot oxidation mechanism different from the 1st-order reaction taking place. It is faster than the 1st-order reaction, consumes about 20% of soot, and is carried out at 120−350 °C. Both consecutive and parallel multi-step reaction models have been used by several researchers to simulate the process consisting of multi-reaction mechanisms.[31,53,54]

Figure 11 shows the prediction of diesel-soot combustion as a function of temperature at different heating rates. The conversion curve shifts toward the right (higher temperature) at an increasing heating rate, but the pattern of the oxidation curve does not change. T_{10} and T_{90} (the temperature corresponding to the soot conversion of 10 and 90%) are also shifted to the higher temperature. It means that higher temperatures are required to start (T_{10}) and finish (T_{90}) the combustion. This information is crucially important, especially when the temperature is abruptly increased caused by the injection of additional diesel fuel directly into the exhaust gas.

https://doi.org/10.1021/acsomega.3c02971
ACS Omega 2023, 8, 29437−29447

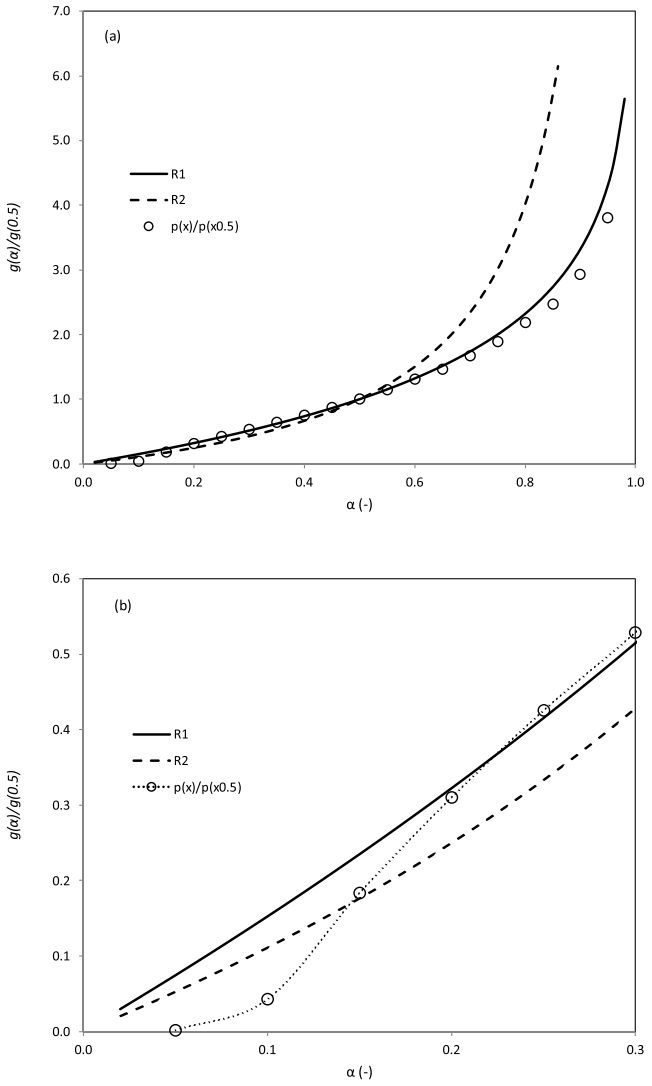

Figure 9. Master plots of $f(\alpha) = (1-\alpha)^n$ and experimental data $p(x)/p(x_{0.5})$ for the soot combustion catalyzed by Ag/Al_2O_3 at the heating rate of 4 °C/min. R1 and R2 stand for n = 1 and 2, respectively; (a) for α from 0 to 1 and (b) for α from 0 to 0.3.

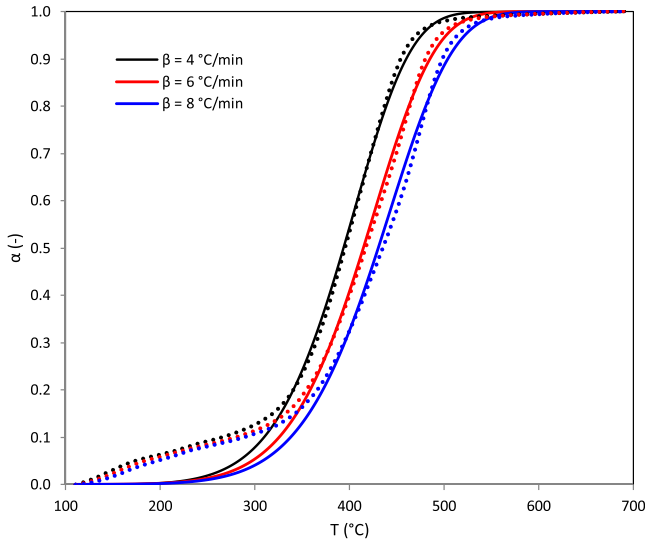

Figure 10. Comparisons between the experiment (dotted lines) and the model (solid lines) at heating rates of 4, 6, and 8 °C/min for the catalytic soot combustion in the presence of Ag/Al_2O_3.

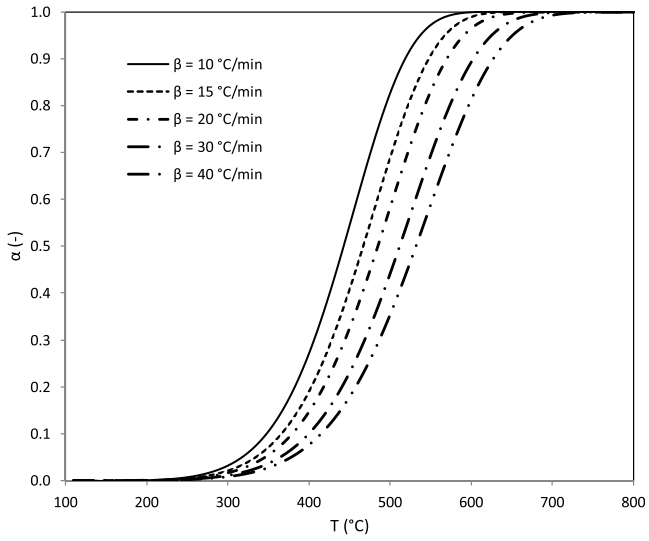

Figure 11. Prediction for the effect of the heating rate on soot combustion in the presence of Ag/Al_2O_3.

The quantity of injected fuel can be estimated to reach the designed regeneration temperature.

Figure 12 shows the prediction of soot conversion as a function of time at different operating temperatures. The figure provides information about the reaction times required to complete the catalytic soot oxidation process. At a relatively high temperature of 500 °C, for example, the catalyst uses 30 min to burn soot completely, while it takes almost 2 h at an exhaust temperature of 400 °C. With Ag/Al_2O_3, the time used to combust soot entirely is much shorter than the oxidation of soot in the absence of a catalyst that needs more than 2 h at the temperature of 500 °C, as shown in Figure 7.

3.4. Soot Oxidation in the Presence of Ag/CeO_2.

Figure 13 demonstrates the distribution of activation energy along the extent of conversion for diesel-soot oxidation accelerated by Ag/CeO_2. The activation energies range between 80 and 120 kJ/mol which is consistent with the values obtained by Gross et al.[55,56] These values are higher than the values obtained from Ag/Al_2O_3, resulting in lower reactivity. Interestingly, at relatively high conversions of 0.85−0.95, the corresponding activation energies are close to the value obtained from the uncatalyzed soot oxidation, indicating that the direct reaction between soot and gas-phase oxygen is dominant at high temperatures. The value of 82.78 kJ/mol is averaged from all computed activation energies and used in the master plots and simulation parts.

With the apparent activation energy obtained previously, the master plots of the reaction-order models, $f(\alpha) = (1-\alpha)^n$, for n of 1 and 2 are plotted and compared to the experimental values, as depicted in Figure 14. Although the 2nd-order model offers higher accuracy at low soot conversion, the 1st-order model gives a proper soot oxidation characteristic for the entire range of conversion. It implies that soot combustion on Ag/CeO_2 consists of a primary reaction mechanism. This combustion behavior contrasts with that carried out on Ag/Al_2O_3 in which at least two reaction mechanisms are needed to explain the catalytic soot oxidation process.

Figure 15 compares the kinetic model with experimental results at heating rates of 2, 4, 6, and 8 °C/min. The proposed

https://doi.org/10.1021/acsomega.3c02971
ACS Omega 2023, 8, 29437−29447

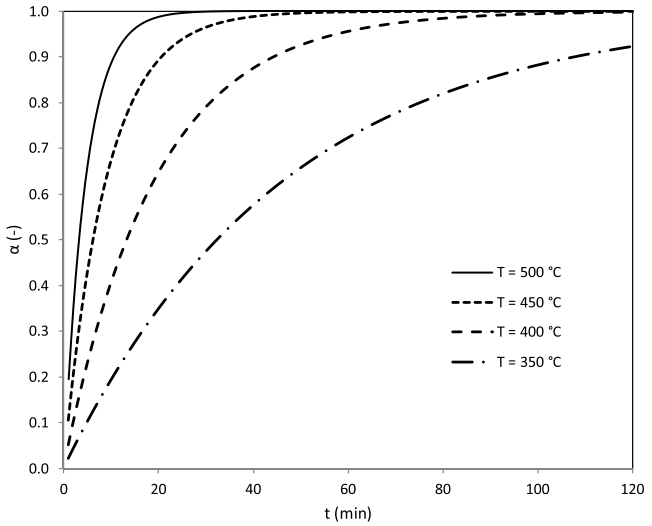

Figure 12. Prediction for the effect of operating temperature on soot combustion in the presence of Ag/Al_2O_3.

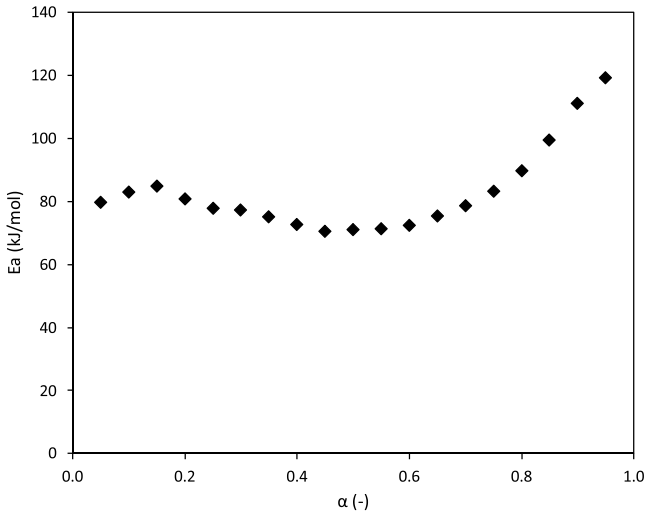

Figure 13. Dependences of the activation energy on the extent of conversion for diesel-soot oxidation in the presence of Ag/CeO_2.

model can successfully predict diesel-soot combustion catalyzed by Ag/CeO_2. The 1st-order reaction model can correctly represent the carbonaceous decomposition for all conversion ranges, indicating that the soot combustion in the presence of Ag/CeO_2 is carried out with only one primary reaction mechanism. In this case, the results implies the absence of additional soot oxidation by oxygen desorbed from Ag/CeO_2 at low temperature region as observed in Ag/Al_2O_3 case.

As the heating rate increases, the temperature at which soot oxidation takes place also increases, resulting in the shifting of soot conversion toward higher temperature when observing at specific soot conversion (e.g., $\alpha = 0.5$), as shown in Figure 16. This is due mainly to the limit of heat transfer from the heat source to the soot particles whose higher heating rate effectively reduces residence time (duration for the soot particle to contact with heat and oxidant) of the soot sample at a given temperature. Additionally, soot particles require a specific duration to completely oxidize. Hence, the soot oxidation reaction at the current moment (in time and temperature) could not be completed, and the process was

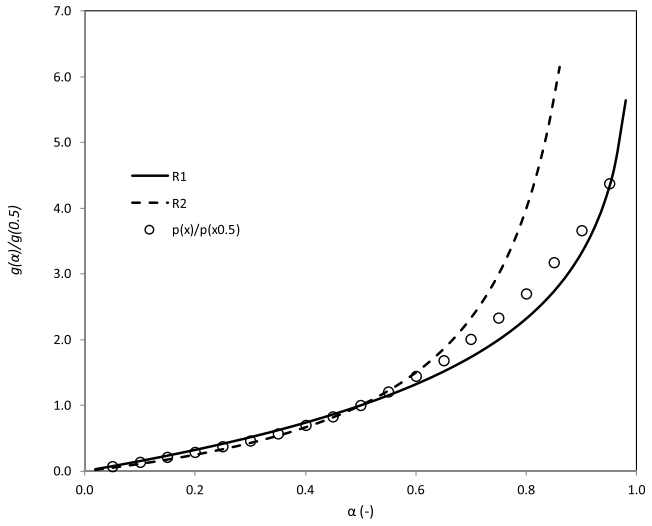

Figure 14. Master plots of $f(\alpha) = (1-\alpha)^n$ and experimental data $p(x)/p(x_{0.5})$ for the soot combustion catalyzed by Ag/CeO_2 at the heating rate of 4 °C/min. R1 and R2 stand for $n = 1$ and 2, respectively.

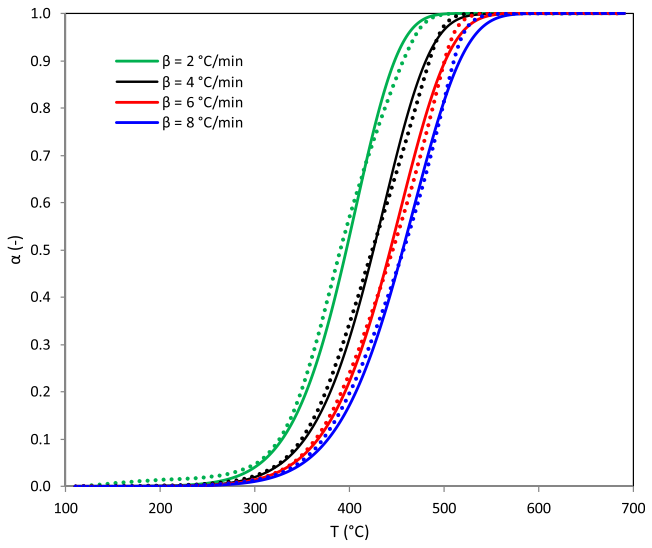

Figure 15. Comparisons between the experiment (dotted lines) and the model (solid lines) at heating rates of 2, 4, 6, and 8 °C/min for the catalytic soot combustion in the presence of Ag/CeO_2.

carried out later where the control boundary temperature has already proceeded to higher temperatures. This heat transfer and oxidation reaction lag phenomenon has been experimentally investigated in previous work by several authors.[57,58]

Figure 17 presents the prediction of diesel-soot conversion in isothermal conditions as a function of time and operating temperature. The figure provides information about the time required for the DPF's regeneration process at a constant temperature. The time used to reach 90% of soot conversion is strongly dependent on the temperature. It takes only 10 min at the exhaust temperature of 500 °C, while it requires more than 1 h at the temperature of 400 °C. Moreover, at the isothermal temperature of 350 °C, there is no chance for Ag/CeO_2 to burn off 90% of soot.

https://doi.org/10.1021/acsomega.3c02971
ACS Omega 2023, 8, 29437−29447

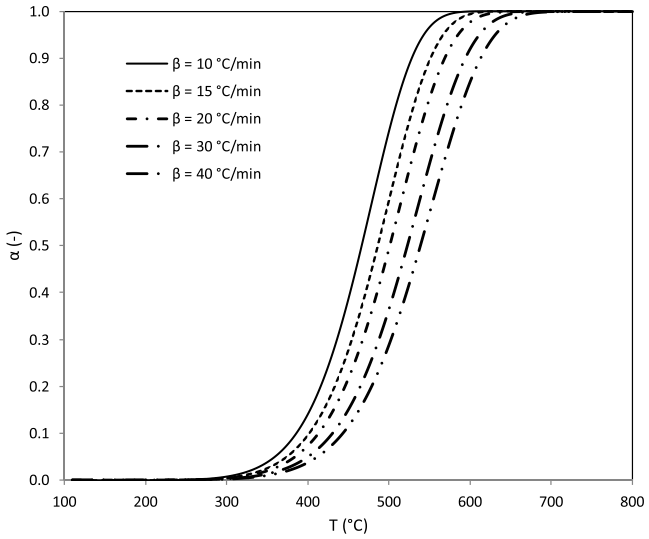

Figure 16. Simulation for the effect of heating rate on soot combustion in the presence of Ag/CeO_2.

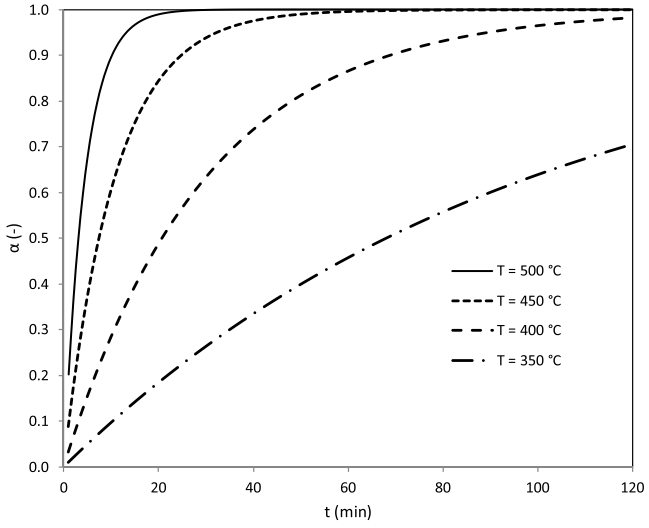

Figure 17. Prediction for the soot conversion as a function of time at different isothermal conditions in the presence of Ag/CeO_2.

4. CONCLUSIONS

This work uses kinetic analysis to investigate the combustion of devolatilized diesel soot in the absence of a catalyst and in the presence of Ag/Al_2O_3 and Ag/CeO_2. The apparent activation energy of the soot combustion is evaluated using the isoconversional approach, and the reaction model is identified using the master-plots technique. In the uncatalyzed soot oxidation, the apparent activation energy is 101.85 kJ/mol, and the combustion proceeds monotonously with a primary reaction mechanism which can be represented by the 1.4th-reaction-order model. In the soot oxidation catalyzed by Ag/Al_2O_3, the apparent activation energy is 61.85 kJ/mol. There is a small amount of highly active oxygen generated by Ag/Al_2O_3 which is desorbed easily at low temperatures in the absence of soot; however, in the presence of soot, this oxygen migrates to soot and consumes around 20% of soot at the temperature between 120 and 350 °C. The reaction mechanism at the beginning of soot burnout is faster than the 1st-order reaction model. The reaction model of the remaining soot (20−100% conversion) can be explained by the 1st-order reaction model. In the presence of Ag/CeO_2, the apparent activation energy for catalytic soot oxidation is 82.78 kJ/mol. The catalyst promotes diesel-soot oxidation at relatively low and medium temperatures, while the direct oxidation between soot and gas-phase oxygen (uncatalyzed combustion) is predominant at relatively high temperatures. The proposed kinetic models can successfully reproduce the data obtained from the experiment and can provide information about temperatures and times required for DPF's regeneration process.

AUTHOR INFORMATION

Corresponding Author

Kampanart Theinnoi − *College of Industrial Technology, King Mongkut's University of Technology North Bangkok, Bangkok 10800, Thailand; Research Centre for Combustion Technology and Alternative Energy (CTAE), Science and Technology Research Institute, King Mongkut's University of Technology North Bangkok, Bangkok 10800, Thailand;* orcid.org/0000-0003-0575-324X; Email: kampanart.t@cit.kmutnb.ac.th

Authors

Boonlue Sawatmongkhon − *College of Industrial Technology, King Mongkut's University of Technology North Bangkok, Bangkok 10800, Thailand; Research Centre for Combustion Technology and Alternative Energy (CTAE), Science and Technology Research Institute, King Mongkut's University of Technology North Bangkok, Bangkok 10800, Thailand;* orcid.org/0000-0001-8972-4387

Punya Promhuad − *College of Industrial Technology, King Mongkut's University of Technology North Bangkok, Bangkok 10800, Thailand*

Thanawat Thaisruang − *College of Industrial Technology, King Mongkut's University of Technology North Bangkok, Bangkok 10800, Thailand*

Sak Sittichompoo − *College of Industrial Technology, King Mongkut's University of Technology North Bangkok, Bangkok 10800, Thailand; Research Centre for Combustion Technology and Alternative Energy (CTAE), Science and Technology Research Institute, King Mongkut's University of Technology North Bangkok, Bangkok 10800, Thailand*

Thawatchai Wongchang − *Research Centre for Combustion Technology and Alternative Energy (CTAE), Science and Technology Research Institute, King Mongkut's University of Technology North Bangkok, Bangkok 10800, Thailand; Department of Mechanical and Automotive Engineering Technology, Faculty of Engineering and Technology, King Mongkut's University of Technology North Bangkok (Rayong Campus), Rayong 21120, Thailand*

Ekarong Sukjit − *School of Mechanical Engineering, Institute of Engineering, Suranaree University of Technology, Nakhon Ratchasima 30000, Thailand;* orcid.org/0000-0003-4641-2580

Complete contact information is available at: https://pubs.acs.org/10.1021/acsomega.3c02971

Notes

The authors declare no competing financial interest.

https://doi.org/10.1021/acsomega.3c02971
ACS Omega 2023, 8, 29437−29447

■ ACKNOWLEDGMENTS

This research was funded by the College of Industrial Technology, King Mongkut's University of Technology North Bangkok (Grant No. Res-CIT0294/2022).

■ REFERENCES

(1) Sawatmongkhon, B.; Theinnoi, K.; Wongchang, T.; Haoharn, C.; Wongkhorsub, C.; Sukjit, E.; et al. Catalytic oxidation of diesel particulate matter by using silver and ceria supported on alumina as the oxidation catalyst. *Appl. Catal. A Gen.* **2019**, *574*, 33−40.
(2) Ramdas, R.; Nowicka, E.; Jenkins, R.; Sellick, D.; Davies, C.; Golunski, S. Using real particulate matter to evaluate combustion catalysts for direct regeneration of diesel soot filters. *Appl. Catal. B* **2015**, *176-177*, 436−443.
(3) Theinnoi, K.; Tsolakis, A.; Sitshebo, S.; Cracknell, R. F.; Clark, R. H. Fuels combustion effects on a passive mode silver/alumina HC-SCR catalyst activity in reducing NOx. *Chem. Eng. J.* **2010**, *158*, 468−473.
(4) Shimizu, K.; Kawachi, H.; Satsuma, A. Study of active sites and mechanism for soot oxidation by silver-loaded ceria catalyst. *Appl. Catal. B* **2010**, *96*, 169−175.
(5) Haneda, M.; Towata, A. Catalytic performance of supported Ag nano-particles prepared by liquid phase chemical reduction for soot oxidation. *Catal. Today* **2015**, *242*, 351−356.
(6) Lee, J. H.; Lee, S. H.; Choung, J. W.; Kim, C. H.; Lee, K.-Y. Ag-incorporated macroporous CeO2 catalysts for soot oxidation: Effects of Ag amount on the generation of active oxygen species. *Appl. Catal. B* **2019**, *246*, 356−366.
(7) Lee, J. H.; Lee, B. J.; Lee, D.-W.; Choung, J. W.; Kim, C. H.; Lee, K.-Y. Synergistic effect of Cu on a Ag-loaded CeO2 catalyst for soot oxidation with improved generation of active oxygen species and reducibility. *Fuel* **2020**, *275*, No. 117930.
(8) Zhang, M.; Jin, B.; Liu, Y.; Liu, W.; Weng, D.; Wu, X.; et al. Ozone activated Ag/CeO2 catalysts for soot combustion: The surface and structural influences. *Chem. Eng. J.* **2019**, *375*, No. 121961.
(9) Wang, H.; Luo, S.; Zhang, M.; Liu, W.; Wu, X.; Liu, S. Roles of oxygen vacancy and Ox− in oxidation reactions over CeO2 and Ag/CeO2 nanorod model catalysts. *J. Catal.* **2018**, *368*, 365−378.
(10) Liu, S.; Wu, X.; Liu, W.; Chen, W.; Ran, R.; Li, M.; et al. Soot oxidation over CeO2 and Ag/CeO2: Factors determining the catalyst activity and stability during reaction. *J. Catal.* **2016**, *337*, 188−198.
(11) Gao, Y.; Duan, A.; Liu, S.; Wu, X.; Liu, W.; Li, M.; et al. Study of Ag/CexNd1-xO2 nanocubes as soot oxidation catalysts for gasoline particulate filters: Balancing catalyst activity and stability by Nd doping. *Appl. Catal. B* **2017**, *203*, 116−126.
(12) Wang, H.; Liu, S.; Zhao, Z.; Zou, X.; Liu, M.; Liu, W.; et al. Activation and deactivation of Ag/CeO2 during soot oxidation: influences of interfacial ceria reduction. *Catal. Sci. Technol.* **2017**, *7*, 2129−2139.
(13) Corro, G.; Vidal, E.; Cebada, S.; Pal, U.; Bañuelos, F.; Vargas, D.; et al. Electronic state of silver in Ag/SiO2 and Ag/ZnO catalysts and its effect on diesel particulate matter oxidation: An XPS study. *Appl. Catal. B* **2017**, *216*, 1−10.
(14) Machida, M.; Murata, Y.; Kishikawa, K.; Zhang, D.; Ikeue, K. On the Reasons for High Activity of CeO2 Catalyst for Soot Oxidation. *Chem. Mater.* **2008**, *20*, 4489−4494.
(15) Corro, G.; Pal, U.; Ayala, E.; Vidal, E. Diesel soot oxidation over silver-loaded SiO2 catalysts. *Catal. Today* **2013**, *212*, 63−69.
(16) Yamazaki, K.; Kayama, T.; Dong, F.; Shinjoh, H. A mechanistic study on soot oxidation over CeO2−Ag catalyst with 'rice-ball' morphology. *J. Catal.* **2011**, *282*, 289−298.
(17) Nanba, T.; Masukawa, S.; Uchisawa, J.; Obuchi, A. Effect of support materials on Ag catalysts used for acrylonitrile decomposition. *J. Catal.* **2008**, *259*, 250−259.
(18) Aneggi, E.; Llorca, J.; de Leitenburg, C.; Dolcetti, G.; Trovarelli, A. Soot combustion over silver-supported catalysts. *Appl. Catal. B* **2009**, *91*, 489−498.
(19) Wang, H.; Luo, S.; Li, X.; Liu, W.; Wu, X.; Weng, D.; et al. Thermally stable Ag/Al2O3 confined catalysts with high diffusion-induced oxidation activity. *Catal. Today* **2019**, *332*, 189−194.
(20) Gao, Y.; Wu, X.; Liu, S.; Ogura, M.; Liu, M.; Weng, D. Aggregation and redispersion of silver species on alumina and sulphated alumina supports for soot oxidation. *Catal. Sci. Technol.* **2017**, *7*, 3524−3530.
(21) Skaf, M.; Aouad, S.; Hany, S.; Cousin, R.; Abi-Aad, E.; Aboukaïs, A. Physicochemical characterization and catalytic performance of 10% Ag/CeO2 catalysts prepared by impregnation and deposition−precipitation. *J. Catal.* **2014**, *320*, 137−146.
(22) Kim, M. J.; Han, G.-H.; Lee, S. H.; Jung, H. W.; Choung, J. W.; Kim, C. H.; et al. CeO2 promoted Ag/TiO2 catalyst for soot oxidation with improved active oxygen generation and delivery abilities. *J. Hazard. Mater.* **2020**, *384*, No. 121341.
(23) Jeguirim, M.; Villani, K.; Brilhac, J. F.; Martens, J. A. Ruthenium and platinum catalyzed carbon oxidation: A comparative kinetic study. *Appl. Catal. B* **2010**, *96*, 34−40.
(24) Zouaoui, N.; Labaki, M.; Jeguirim, M. Diesel soot oxidation by nitrogen dioxide, oxygen and water under engine exhaust conditions: Kinetics data related to the reaction mechanism. *C. R. Chim.* **2014**, *17*, 672−680.
(25) Zouaoui, N.; Issa, M.; Kehrli, D.; Jeguirim, M. CeO2 catalytic activity for soot oxidation under NO/O2 in loose and tight contact. *Catal. Today* **2012**, *189*, 65−69.
(26) Azambre, B.; Collura, S.; Darcy, P.; Trichard, J. M.; Da Costa, P.; García-García, A.; et al. Effects of a Pt/Ce0.68Zr0.32O2 catalyst and NO2 on the kinetics of diesel soot oxidation from thermogravimetric analyses. *Fuel Process. Technol.* **2011**, *92*, 363−371.
(27) Leistner, K.; Nicolle, A.; Berthout, D.; Costa, P. Kinetic modelling of the oxidation of a wide range of carbon materials. *Combust. Flame* **2012**, *159*, 64−76.
(28) Leistner, K.; Nicolle, A.; Da Costa, P. Detailed Kinetic Analysis of Soot Oxidation by NO2, NO, and NO + O2. *J. Phys. Chem. C* **2012**, *116*, 4642−4654.
(29) Leistner, K.; Nicolle, A.; Da Costa, P. Impact of the Catalyst/Soot Ratio on Diesel Soot Oxidation Pathways. *Energy Fuels* **2012**, *26*, 6091−6097.
(30) Galwey, A. K., Brown, M. E. Kinetic background to thermal analysis and calorimetry. In *Handbook of thermal analysis and calorimetry Volume 1 Principles and practice*, Brown, M. E., Ed.; 1998, pp. 147−224.
(31) Gross, M. S.; Sánchez, B. S.; Querini, C. A. Diesel particulate matter combustion with CeO2 as catalyst. Part II: Kinetic and reaction mechanism. *Chem. Eng. J.* **2011**, *168*, 413−419.
(32) Vyazovkin, S.; Burnham, A. K.; Criado, J. M.; Pérez-Maqueda, L. A.; Popescu, C.; Sbirrazzuoli, N. ICTAC Kinetics Committee recommendations for performing kinetic computations on thermal analysis data. *Thermochim. Acta* **2011**, *520*, 1−19.
(33) Bartocci, P.; Tschentscher, R.; Stensrød, R. E.; Barbanera, M.; Fantozzi, F. Kinetic Analysis of Digestate Slow Pyrolysis with the Application of the Master-Plots Method and Independent Parallel Reactions Scheme. *Molecules* **2019**, *24*, 1657.
(34) Sánchez-Jiménez, P. E.; Pérez-Maqueda, L. A.; Perejón, A.; Criado, J. M. Generalized master plots as a straightforward approach for determining the kinetic model: The case of cellulose pyrolysis. *Thermochim. Acta* **2013**, *552*, 54−59.
(35) de Carvalho, V. S.; Tannous, K. Thermal decomposition kinetics modeling of energy cane Saccharum robustum. *Thermochim. Acta* **2017**, *657*, 56−65.
(36) Luo, L.; Zhang, Z.; Li, C.; Nishu, H. F.; Zhang, X.; et al. Insight into master plots method for kinetic analysis of lignocellulosic biomass pyrolysis. *Energy* **2021**, *233*, No. 121194.
(37) López-Fonseca, R.; Elizundia, U.; Landa, I.; Gutiérrez-Ortiz, M. A.; González-Velasco, J. R. Kinetic analysis of non-catalytic and Mn-catalysed combustion of diesel soot surrogates. *Appl. Catal. B* **2005**, *61*, 150−158.

https://doi.org/10.1021/acsomega.3c02971
ACS Omega 2023, 8, 29437−29447

(38) López-Fonseca, R.; Landa, I.; Elizundia, U.; Gutiérrez-Ortiz, M. A.; González-Velasco, J. R. A kinetic study of the combustion of porous synthetic soot. *Chem. Eng. J.* **2007**, *129*, 41−49.
(39) Song, Q.; He, B.; Yao, Q.; Meng, Z.; Chen, C. Influence of Diffusion on Thermogravimetric Analysis of Carbon Black Oxidation. *Energy Fuels* **2006**, *20*, 1895−1900.
(40) Sharma, H. N.; Pahalagedara, L.; Joshi, A.; Suib, S. L.; Mhadeshwar, A. B. Experimental Study of Carbon Black and Diesel Engine Soot Oxidation Kinetics Using Thermogravimetric Analysis. *Energy Fuels* **2012**, *26*, 5613−5625.
(41) White, J. E.; Catallo, W. J.; Legendre, B. L. Biomass pyrolysis kinetics: A comparative critical review with relevant agricultural residue case studies. *J. Anal. Appl. Pyrolysis* **2011**, *91*, 1−33.
(42) Fedunik-Hofman, L.; Bayon, A.; Donne, S. W. Kinetics of Solid-Gas Reactions and Their Application to Carbonate Looping Systems. *Energies* **2019**, *12*, 2981.
(43) Janković, B. Kinetic analysis of the nonisothermal decomposition of potassium metabisulfite using the model-fitting and isoconversional (model-free) methods. *Chem. Eng. J.* **2008**, *139*, 128−135.
(44) Vyazovkin, S. Computational aspects of kinetic analysis. Part C. The ICTAC Kinetics Project - the light at the end of the tunnel? *Thermochim. Acta* **2000**, *355*, 155.
(45) Starink, M. J. The determination of activation energy from linear heating rate experiments: a comparison of the accuracy of isoconversion methods. *Thermochim. Acta* **2003**, *404*, 163−176.
(46) Sbirrazzuoli, N. Determination of pre-exponential factors and of the mathematical functions f(α) or G(α) that describe the reaction mechanism in a model-free way. *Thermochim. Acta* **2013**, *564*, 59−69.
(47) Ganiger, S.; Patil, S. S.; Dasari, H. P.; Priyanka, R.; Kollimarla, S. Printex-U soot oxidation kinetic behaviour over Alumina and Quartz. *Chem. Eng. Sci.* **2022**, *247*, No. 117016.
(48) López-Fonseca, R.; Landa, I.; Elizundia, U.; Gutiérrez-Ortiz, M. A.; González-Velasco, J. R. Thermokinetic modeling of the combustion of carbonaceous particulate matter. *Combust. Flame* **2006**, *144*, 398−406.
(49) Gotor, F. J.; Criado, J. M.; Malek, J.; Koga, N. Kinetic Analysis of Solid-State Reactions: The Universality of Master Plots for Analyzing Isothermal and Nonisothermal Experiments. *J. Phys. Chem. A* **2000**, *104*, 10777−10782.
(50) Málek, J.; Koga, N.; Pérez-Maqueda, L. A.; Criado, J. M. The Ozawa's generalized time concept and YZ-master plots as a convenient tool for kinetic analysis of complex processes. *J. Therm. Anal. Calorim.* **2013**, *113*, 1437−1446.
(51) Zouaoui, N.; Brilhac, J. F.; Mechati, F.; Jeguirim, M.; Djellouli, B.; Gilot, P. Study of experimental and theoretical procedures when using thermogravimetric analysis to determine kinetic parameters of carbon black oxidation. *J. Therm. Anal. Calorim.* **2010**, *102*, 837−849.
(52) Kalogirou, M.; Samaras, Z. Soot oxidation kinetics from TG experiments. *J. Therm. Anal. Calorim.* **2010**, *99*, 1005−1010.
(53) di Sarli, V.; di Benedetto, A. Modeling and simulation of soot combustion dynamics in a catalytic diesel particulate filter. *Chem. Eng. Sci.* **2015**, *137*, 69−78.
(54) Landi, G.; di Sarli, V.; Lisi, L. A Numerical Investigation of the Combined Effects of Initial Temperature and Catalyst Activity on the Dynamics of Soot Combustion in a Catalytic Diesel Particulate Filter. *Top. Catal.* **2021**, *64*, 270−287.
(55) Gross, M. S.; Ulla, M. A.; Querini, C. A. Diesel particulate matter combustion with CeO2 as catalyst. Part I: System characterization and reaction mechanism. *J. Mol. Catal. A: Chem.* **2012**, *352*, 86−94.
(56) Gross, M. S.; Ulla, M. A.; Querini, C. A. Catalytic oxidation of diesel soot: New characterization and kinetic evidence related to the reaction mechanism on K/CeO2 catalyst. *Appl. Catal. A Gen.* **2009**, *360*, 81−88.
(57) Rodríguez-Fernández, J.; Oliva, F.; Vázquez, R. A. Characterization of the Diesel Soot Oxidation Process through an Optimized Thermogravimetric Method. *Energy Fuels* **2011**, *25*, 2039−2048.
(58) Pu, P.; Fang, J.; Zhang, Q.; Yang, Y.; Qin, Z.; Meng, Z.; et al. Effect of Operating Parameters on Oxidation Characteristics of Soot under the Synergistic Action of Soluble Organic Fractions and Ash. *ACS Omega* **2021**, *6*, 17372−17378.

https://doi.org/10.1021/acsomega.3c02971
ACS Omega 2023, 8, 29437−29447